Journal of Applied Electrochemistry **30**: 803–807, 2000.

A new technique for two-dimensional current distribution measurements in electrochemical cells

Ch. WIESER, A. HELMBOLD and E. GÜLZOW
Institut für Technische Thermodynamik, Deutsches Zentrum für Luft- und Raumfahrt, Pfaffenwaldring 38-40, 70569 Stuttgart, Germany

Received 22 March 1999; accepted in revised form 4 January 2000

Key words: current distribution, electrochemical cell, fuel cell

Abstract

A new technique has been developed using a magnetic loop array to measure current distribution in electrochemical cells. The main advantage of this approach is the combination of high spatial and time resolution and stack integration with an easily handled measurement carried out independently of the cell operation. A polymer electrolyte fuel cell (PEFC) of technically relevant dimensions (about 600 cm^2 electrode area) with 5×8 current sensors has been constructed and operated, thus confirming the feasibility of the measurement technique.

1. Introduction

Obstacles to the commercialization of fuel cells, such as reducing catalyst loadings, improving membrane materials and using hydrocarbon fuels, have been overcome to a large extent leading to high performing laboratory fuel cells [1, 2]. Scaling these cells to commercial dimensions is accompanied by significant performance losses caused, for example, by local mass transport effects, unevenly manufactured electrode membrane assemblies, locally varying contact resistances and temperature gradients leading to uneven current distributions.

To exploit the potential informational content of current distribution measurements the following requirements should be fulfilled:

(i) being the object of measurement, the electrode membrane assembly (EMA) should not have to be modified
(ii) high spatial resolution across the entire electrode area to cover possible steep current gradients
(iii) high time resolution to allow current mapping during dynamic operation
(iv) measurement independent of fuel cell operation
(v) optional integration of the measurement cell into a fuel cell stack with large electrode areas.

To date, most approaches performing current distribution measurements in the PEFC are based on investigations in electrolysers. At the Los Alamos National Laboratory (LANL) the printed circuit board (PCB) approach, as already applied by Brown et al. [3], has been adapted to a 100 cm^2 PEFC [4]. Recently, Stumper et al. [5] presented results using the partial MEA approach, the microelectrode approach [6] in a subcell design, as well as a modified segmented current collector design [7] for current distribution mapping in a 240 cm^2 cell [5].

Although a good spatial resolution can be obtained by the PCB approach, real two-dimensional current mapping with inner segments is difficult. Dividing the cell into strip shaped segments requires a corresponding segmentation of the gas diffusion electrode to avoid undesired lateral currents due to varying contact and conduction resistances. The restriction on two electronic loads which complementarily scan the segments leads to load transients interfering with cell operation. Additional sensing wires are required to synchronize the individual segment potentials. To integrate the measurement cell into a stack, where the individual cell voltages normally float freely, a control loop to split the stack current is inevitable to meet the necessary potential synchronization.

The practicability of the partial MEA approach depends substantially on the reproducibility of the MEA preparation and cell performance stability. Thus it is questionable if the avoidance of special equipment compensates for the high preparation expenditure and the moderate spatial resolution.

The further development of the microelectrode approach in a subcell design by two microelectrodes arranged face to face allows the distinction between cathode and anode performance. To achieve this a careful alignment of the corresponding electrode areas is necessary. Despite the high preparative expenditure for the flowfield/current collector, as well as for the EMA, uncertainties about the overlaped electrode area cannot be excluded. If the uncovered area surrounding the subcell is large compared with the subcell area the local mass transport and membrane humidification might be influenced.

For current mapping of the entire electrode area simplifying approaches are necessary. Stumper et al. used a passive resistor network made from resin isolated graphite blocks located between the flowfield and current collector. By measuring the voltage drop across each graphite shunt the local current through the corresponding cross section of the cell can be monitored and by scanning the entirety of the segments the current distribution can be obtained. The main problem of the published configuration arises from the omission of the flowfield segmentation. Due to a disadvantageous ratio of lateral versus perpendicular conductivities, significant lateral currents cannot be avoided. Presuming the conductivity of the flowfield is determined, this ratio can only be decreased by lowering the shunt and contact resistances. Obviously, the shunt resistance cannot be reduced arbitrarily. Furthermore, in the case of low shunt resistances, the influence of varying contact resistances must not be neglected as suggested by the scatter in current distribution in [5].

To avoid these limitations, which mainly depend on the necessity of modifying the current path normal to the cell area, we have developed an advanced technique using a contactless magnetic loop array for sensing local currents [8]. The functionality of this approach has been demonstrated in a large electrode area PEFC (578 cm^2) divided into 40 segments.

2. Principle of measurement

The magnetic field surrounding electric currents allows for the indirect determination of the current (I) by measuring the magnetic induction (B):

$$B = \frac{\mu_0}{2\pi r} I \tag{1}$$

where $\mu_0 = 1.256 \times 10^{-6}$ V s A^{-1} m^{-1} represents the magnetic field constant and r is the distance from the center of the straight current conductor. In contrast to other devices, such as magneto resistors, Hall sensors are well suited for magnetic field measurements because they are sufficiently sensitive but provide a linear output voltage characteristic with regard to the magnetic induction B

$$U_{\text{Hall}} = cI_{\text{Hall}}B \tag{2}$$

where c is a sensor dependant constant and I_{Hall} represents the sensor supply current. To increase the sensitivity of the current measurement the Hall sensor is placed in a slit in an annular soft magnetic material with a high relative permeability μ_r surrounding the current path. With common relative permeabilities of $\mu_r > 1000$ the gain in signal will be

$$\frac{2\pi r}{\partial} \tag{3}$$

where ∂ is the width of the airgap. Assuming a radius of the magnetic loop of 1 cm and an airgap of 0.7 mm in anticipation of the actual design a gain of almost two decades can be obtained. Because of the decrease in the magnetic induction with distance according to Equation 1 this gain is high enough to reduce the influence of adjacent current paths. A schematic drawing of the arrangement is shown in Figure 1. In the following we will call this assembly of magnetic loop and the enclosed Hall sensor a current sensor.

To meet the requirements of the operation of a current sensor integrated in an electrochemical cell a careful selection of the components used is necessary. As a Hall sensor we chose a Siemens KSY44 because of the following characteristics [9]:

(i) low temperature coefficient of the open circuit Hall voltage (about -0.03% K^{-1})
(ii) low ohmic offset voltage ($\leq \pm 15$ mV)
(iii) high sensitivity (1.5–2.3 V T^{-1})
(iv) sufficiently high operating temperature limitation (175 °C)
(v) small dimensions: low thickness (0.7 mm) and small package area (2.1 mm × 3 mm)

An appropriate soft magnetic material for the loop must combine a sufficiently high permeability with a low hysteresis such as soft magnetic metals and soft ferrites. While soft magnetic metals can be conventionally machined and easily adapted to the specific geometric requirements of the current sensor in the cell, they need an extensive annealing process in hydrogen atmosphere above 1000 °C to reach the low hysteresis value of good soft ferrites. Thus we have used annular soft ferrites (Siemens Siferrit R36–N30) with a sufficiently high curie temperature of 130 °C in our current sensors. The slit for the Hall sensor was cut with a diamond wire saw. The characteristic Hall voltage against current curves of current sensors using the Siemens KSY44 Hall sensor with one of the best available metallic (VAC Vacoperm 100) and the used ferritic soft magnetic material are shown in Figure 2. The different sensitivities of the

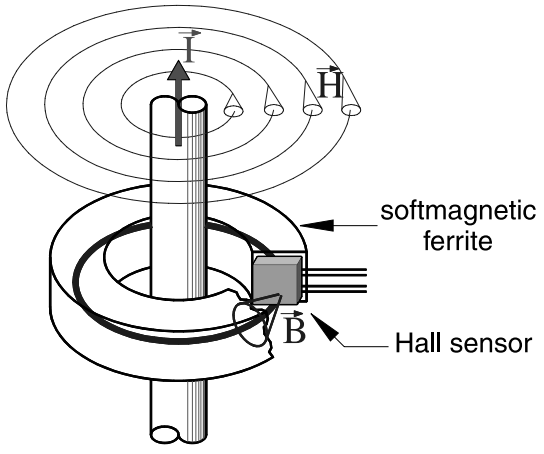

Fig. 1. Schematic drawing of a current sensor with magnetic loop and hall sensor shown with magnetic field generating electric current.

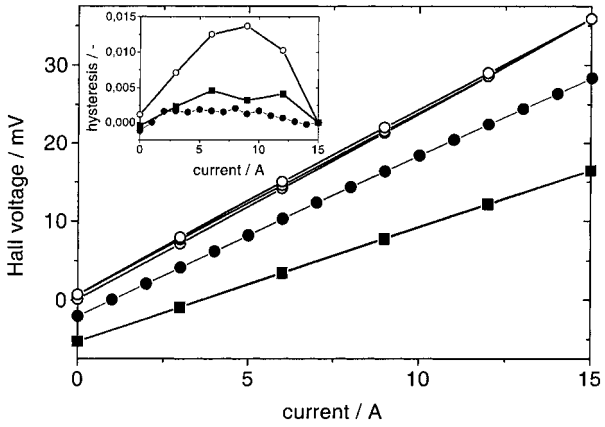

Fig. 2. Characteristic curves of current sensors using the Siemens KSY44 Hall sensor with VAC Vacoperm 100 as delivered and after final treatment and Siemens Siferrit R36–N30. The inset shows the hysteresis as Hall voltage difference normalized with the maximum hall sensor output difference at $I = 15$ A. Key: (■) Siferrit R36–N30; (○) VAC Vacoperm 100 untreated; (●) VAC Vacoperm 100 H_2-tempered.

current sensors, as defined by the slope of the characteristic curves, is not only due to the varying Hall sensor sensitivities but also to different slit widths caused by the manufacturing process.

As well as the remaining hysteresis, another main error in measurement is due to the temperature dependence of the current sensor. Assuming a linear characteristic of the Hall sensor, the influence of the temperature is reflected by a temperature dependant offset voltage and a temperature dependant sensitivity. Examples of these dependencies for a current sensor sample are shown in Figures 3 and 4.

An approximately linear decrease in sensitivity with increasing temperature is observed. From the linear regression a temperature coefficient of $-0.07\%\ K^{-1}$ was measured, which is over two times as high as specified by the manufacturer, suggesting an influence of the ferrite. A negative temperature coefficient of the ferrite permeability would explain the discrepancy. Indeed, over a restricted temperature range some ferrites show such a negative coefficient but in general the permeabilitiy increases with temperature as long as the curie temper-

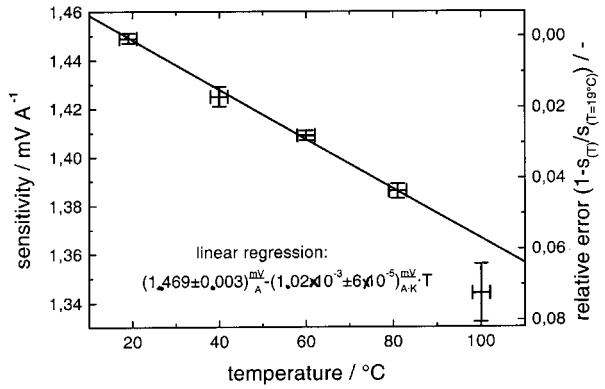

Fig. 3. Total and relative sensitivity of current sensor with temperature.

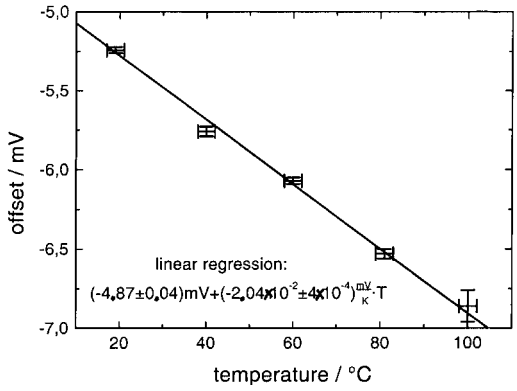

Fig. 4. Offset of current sensor with temperature.

ature is not reached. Assumed the temperature coefficient of the ferrite used for the loop is negative, a conservative calculation with a value of $0.3\%\ K^{-1}$ shows that the above mentioned deviation can only be explained by the influence of the ferrite if its permeability is below 1000. However, this ferrite is characterized by the manufacturer with a positive temperature coefficient over the whole temperature range, as well as with a relative initial permeability greater than 4000 above room temperature. Another explanation might be the variation of the gap by thermal expansion. Nevertheless, we would expect a gap reduction with increasing temperature and hence an increase in sensitivity. After the installation of the current sensors, measurements of the temperature dependence of a new batch of Hall sensors showed no deviation from the specification. The temperature dependence of the Hall sensor sensitivity is mainly determined by the temperature dependence of the Hall coefficient and is thus very sensitive to the Hall sensor material and its purity. In contrast, the temperature dependence of the offset voltage is mainly determined by the temperature dependence of the ohmic resistance and device symmetry. Particularly at low currents the overall temperature dependence of the current sensor is dominated by the temperature dependence of the offset. A simple comparison of the slope coefficients shows that at a current of 1 A the temperature influence of the offset is twenty times that of the sensitivity. Of course at 20 A the influence of both is comparable.

Long term stability investigations were performed with a separate current sensor held at 80 °C in a laboratory oven for 14 days with a testing current of 15 A. The Hall signal deviation was below 1% and corresponds well with the variation of the simultaneously measured internal resistance of the Hall sensor indicating the influence of temperature variation in the oven.

3. Cell configuration

To observe distinct effects, a large PEFC with an active area of 19.0 cm × 30.4 cm (578 cm^2) was designed. To avoid lateral currents in the titanium flowfield it was

segmented. In principle the electrode has to be segmented, too. Because of the more than two decades lower specific conductivity of the gas diffusion layer and the small cross section the lateral currents therein can be neglected if the segments are sufficiently large. Therefore, we chose a segment size of 38 mm × 38 mm resulting in a 5 × 8 matrix of 40 square segments minimizing the ratio of circumference and area. Measurements of the lateral currents in the electrode showed that the error in measurement of the current gradient between neighbouring segments was below 5%. This error was strongly influenced by the contact pressure. The current sensor was placed around the gudgeon of the flowfield segment (Figure 5) which was fixed on the bipolar measurement frame with a counter-sunk screw minimizing additional contact resistances. The angle between the Hall sensor position and the segment border was 45° to ensure a maximum distance of Hall sensor and neighbouring segments. This position also simplified the wiring of the Hall sensors through the side of the measurement frame. The entire hollow space in the current sensor array was cast gas-tight with silicon, which also electrically isolated the segments. The thickness of the measurement frame was mainly determined by the width of the Hall sensor and the necessary thickness of the flowfield. Because no ferrites with appropriate dimensions of 3 mm thickness were commercially available a thicker Siferrit R36 was sliced and a 1 mm radial gap for the Hall sensor was cut. The overall thickness of the actual measurement frame was 10 mm.

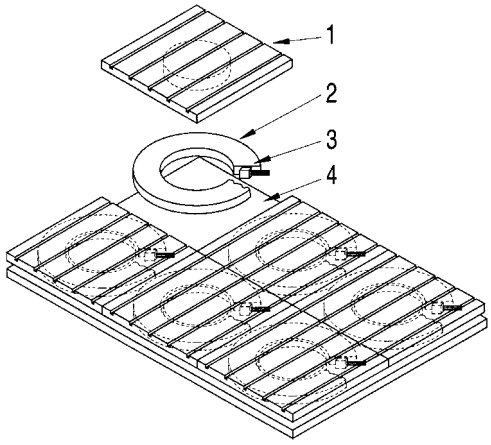

Fig. 5. Schematic figure of current sensor in current collector with flow field segment: (1) flow field segment, (2) annular ferrite, (3) Hall sensor and (4) current collector.

The segmented flowfield comprised straight channels of 1×1 mm^2 cross section with a spacing of 4.8 mm. The unsegmented flow field under investigation was inserted into the counter electrode current collector. First investigations were undertaken with the same flowfield design at the counter electrode side.

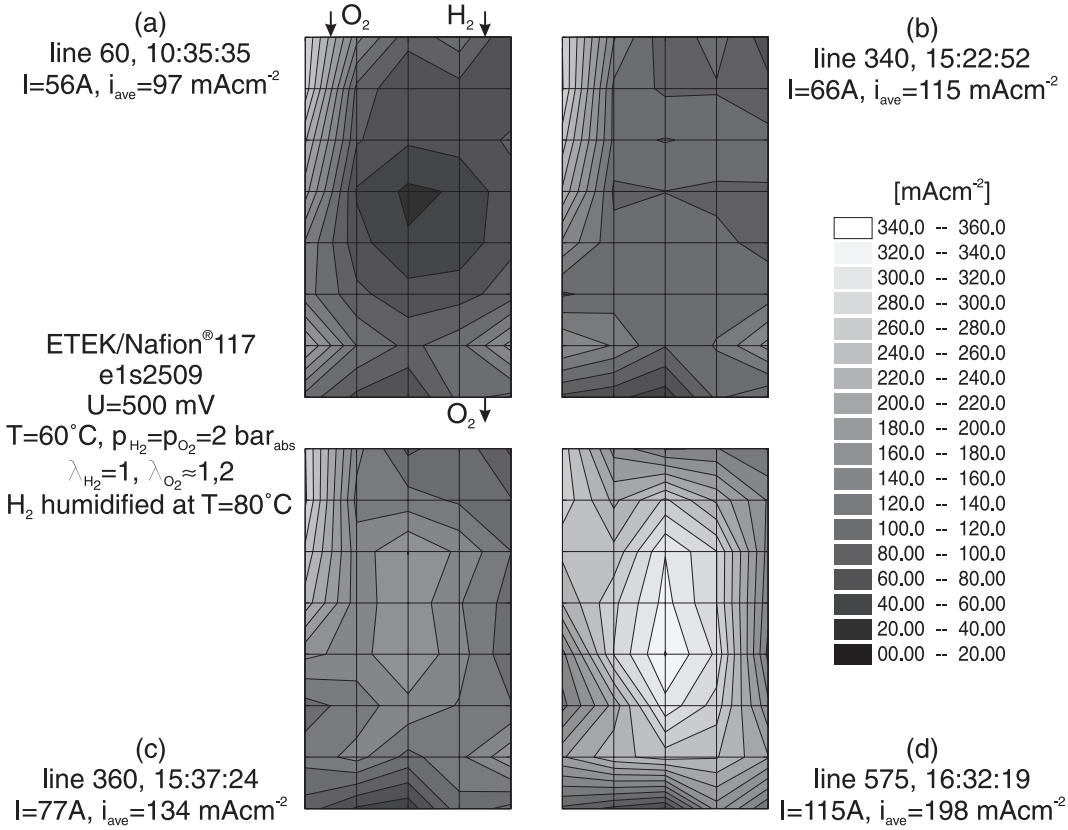

Fig. 6. Change of current density distribution from starting up (picture (a)) with increasing mounting pressure in the center of the cell (pictures (b)–(d)). While the points of measurement are represented by the intersections of the grid lines intermediate values are calculated by linear interpolation.

4. Measurement set-up

Each Hall sensor was supplied with a constant Hall current of 7 mA by a separate constant current source. The 40 Hall sensor voltages were measured using a HP 3852 data acquisition unit equipped with multiplexers and an integrating voltmeter. The HP mainframe was connected to a PC for data acquisition and online visualization. Using an integration time of one linecycle the time for a complete scan including data acquisition and visualization was less than three seconds. For this integration time a typical noise was 1 mA cm^{-2}. Reducing the integration time to 2 ms led to a scanning time of about one second but increased the noise by one decade.

5. Example of operation and discussion

The benefit of current mapping measurements in electrochemistry is not limited to flow field investigations. Although this was the main incentive we demonstrated the operability of our technique by a sequence of measurements showing the influence of the cell bracing.

For later investigations of the cathode with different flow fields the measurement frame was mounted at the anode. The EMA comprised a Nafion^{TM}117 membrane between two ETEK/ELAT electrodes with 0.4 mg cm^{-2} platinum loading (20 wt% Pt on carbon black). The EMA was hot-pressed at 160 °C for three minutes under 80 bar pressure. The cell was mounted between two tempering plates and two bracing plates which were equipped with arrays of screws to allow local variation of the mounting pressure. The bracing plates were 12 mm thick and reinforced with bars (20×40 mm^2 cross section). Finally, the cell was installed into a computer controlled test setup. The cell temperature was held at 60 °C by water circulation from a tempering bath through the tempering plates. The operating pressure was 2 $bar_{(abs)}$ on both sides. The hydrogen gas was water vapour saturated at 80 °C and stoichiometrically fed to the cell. The reaction water was removed by cyclical purging of the cathode with unhumidified oxygen resulting in an effective oxygen stoichiometry below 1.2. The cell potential was held constant at 500 mV by an electronic load.

After start up a current density distribution with increasing local currents from the center of the cell to its border as shown in Figure 6(a) was observed. Considering the large dimensions of the cell this might be caused by the bracing over the border (Figure 7). To verify this assumption the inner bracing plate screws were tightened (Figures 6(b–d)) leading to a drastic increase in overall current and especially in local current density in the cell center. This example clearly demonstrates the strong influence of such bracing effects on the local electrochemical performance. Furthermore, disregarding such effects could lead to wrong interpretations of current density distributions if only mass transport aspects are considered.

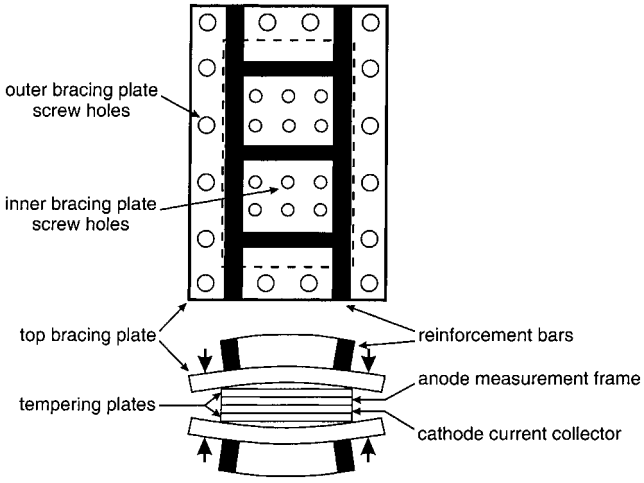

Fig. 7. Schematic drawing of cell bracing. In the side view the elastic deformation of the bracing plate due to the force by the outer bracing screws is emphasized.

Acknowledgements

The authors acknowledge the assistance of Torsten Kraft in measuring the current distribution.

References

1. K.S. Dhathathreyan, P. Sridhar, G. Sasikumar, K.K. Ghosh, G. Velayutham, N. Rajalakshmi, C.K. Subramaniam and K. Ramya, *Int. J. Hydrogen Energy* **24** (1999), 1107–1115.
2. T.R. Ralph, *Platinum Metals Rev.* **41**(3) (1997) 102–113.
3. C.J. Brown, D. Pletcher, F.C. Walsh, J.K. Hammond and D. Robinson, *J. Appl. Electrochem.* **22** (1992) 613–619.
4. S.J.C. Cleghorn, C.R. Derouin, M.S. Wilson and S. Gottesfeld, *J. Appl. Electrochem.* **28** (1998) 663–672.
5. J. Stumper, S.A. Campbell, D.P. Wilkinson, M.C. Johnson and M. Davis, *Electrochim. Acta* **43** (1998) 3773–3783.
6. A.A. Wragg and A.A. Leontaritis, *Dechema Monograph* **123** (1992) 345–360.
7. F. Goodridge, G.M. Mamoor and R.E. Plimley, *I. Chem. E. Symp. Ser.* **98** (1985) 59–69.
8. German Patent Application *Nr. 197 50 738* (15 Nov. 1998).
9. Siemens Magnetic Sensors Data Book 08.95 (Siemens AG, 1995).